Compositional and Microstructural Profiles across Nb_3Sn Filaments Produced by Different Fabrication Methods

P. J. Lee and D. C. Larbalestier

Abstract— **The next generation of high field magnets for fusion and accelerator applications requires the development of Nb_3Sn strand with significantly higher critical current densities. Our recent work has shown that when the specific pinning force is normalized to the grain boundary density (the primary pinning site in this material), a strong increase in pinning force is observed for high Sn content strand, suggesting a strong compositional dependency for pinning in this material. In this study we use advanced FESEM techniques to quantify the compositional and microstructural variations to a sub-100 nm level. A stepped compositional and microstructural variation was observed across a bronze-processed Nb_3Sn filaments with sharp interfaces for both Cu(Sn)-Nb_3Sn and Nb_3Sn-Nb. Microstructural variation was observed on the scale of the original filaments in high Sn, MJR but not across the coalesced filament mass. A very high microstructural uniformity was observed in a PIT monofilament. Thus a major influence of Sn appears to be exerted through its influence on the composition gradient.**

Index Terms—**niobium-tin compounds, microstructure, critical current, composition gradient**

I. Introduction

A significant increase in the critical current density of Nb_3Sn is required for both medium and high field VLHC options - are we already close enough to perfection that significant improvements can not be expected?

The high energy physics led development of Nb-Ti has resulted in a commodity, commercial product available in long lengths at low cost from a number of highly competitive companies. For Nb-Ti:

1. With the exception of a small region at the edge of the filaments the microstructure is homogeneous across each filament.
2. The micro-structure/chemistry is uniform from filament to filament.
3. The filaments are uniform in shape and size and are

Manuscript received September 17, 2000. This work was supported by the US Dept. of Energy, Office of Fusion Energy Sciences, DE-FG02-86ER52131 and Division of High Energy Physics, DE-FG02-91ER40643, and also benefited from NSF-MRSEC DMR-9632427 supported facilities.

Peter J. Lee and D. C. Larbalestier are from Applied Superconductivity Center, University of Wisconsin-Madison, Madison, WI. D. C. Larbalestier is also with the Department of Materials Science and Engineering, University of Wisconsin-Madison.

Contact: Peter J. Lee, The Applied Superconductivity Center, The University of Wisconsin-Madison, 939 ERB, 1500 Engineering Drive, Madison, WI 53706-1687. Email: lee@engr.wisc.edu

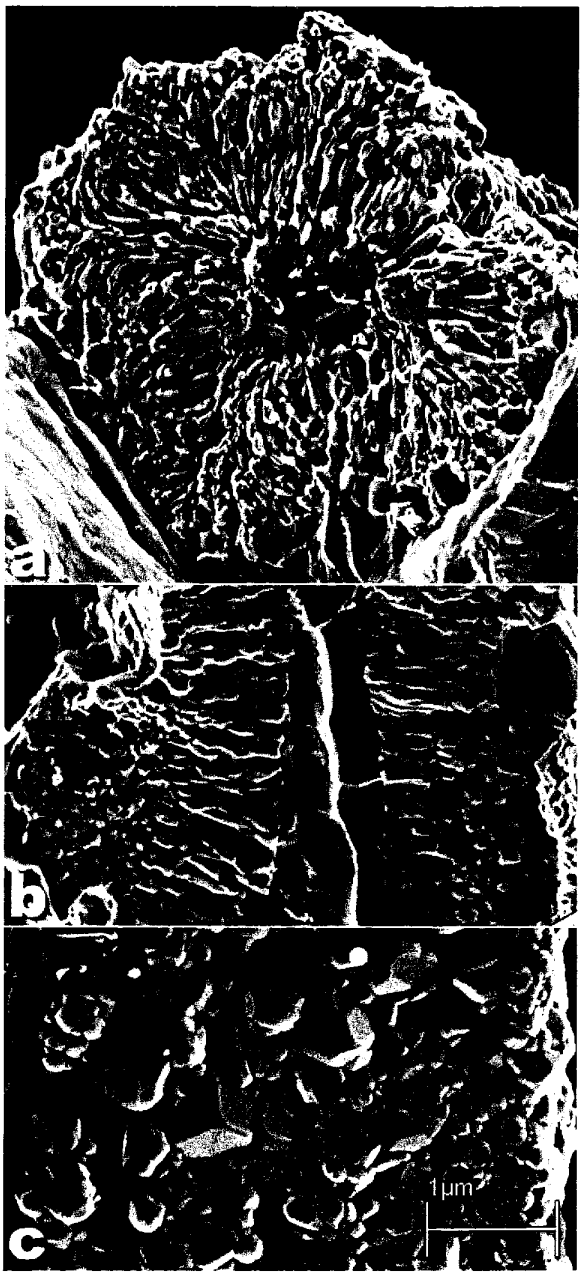

Fig. 1. FESEM fractographs revealing a) Transverse cross-section, b) longitudinal cross-section and c) filament-surface microstructure in a bronze-process Vacuumschmelze ITER strand.

uncoupled.

4. The role of chemistry, heat treatment, and processing on the J_c is well understood and well controlled.

The contrast between Nb_3Sn and Nb-Ti is quite striking:

1. The microstructure is inhomogeneous across each and every filament (e.g. [1]).
2. The micro-structure/chemistry generally varies with filament position (e.g. [1]-[4]).
3. The filaments are generally irregular in shape and size and become more coupled as superconductor volume in the cross-section increases (e.g. [5]).
4. The role of chemistry, heat treatment and processing on J_c, or H_{c2}, or H^* or T_c is not well understood and is thus largely uncontrolled.

The task of understanding the influences of processing variables is complicated by the complexity of the Nb-Sn system and the inhomogeneity of the strands. In this paper we examine aspects of the microstructural and chemical inhomogeneity for bronze and internal tin MJR conductors.

II. Experimental Procedure

A. Microstructure

The inhomogeneity of Nb_3Sn composites provides a considerable challenge to microstructural characterization because of variations within filaments and from filament to filament. The location within the strand cross-section and within the filament must be known and numerous analyses must be performed in order to assess this variation. Traditional analysis by Transmission Electron Microscopy, TEM is then exceptionally laborious and difficult because of the difficulty in preparing a full-filament, electron-transparent cross-section, while retaining location information of that filament. Recent advances in the resolution of Field Emission Scanning Electron Microscopes, however, have made it possible to reliably quantify the microstructure of A15 phases by fractography [1]. Fig. 1 shows FESEM fractographs of a bronze process ITER-VAC strand after a standard ITER heat treatment. The contrasts are quite striking between the transverse and longitudinal cross-sections and the grain size at the filament surface. In order to show the variation in microstructure with position we use a process of position normalization. Each analyzed microstructural feature is located with respect to its distance from the filament centroid and the closest reaction interface.

B. Composition

We have recently extended the position normalization technique to Backscattered Electron Imaging, BEI, in the FESEM, in order to observe chemical changes at a resolution below 100nm [6].

The potential for applying backscattered electron spectroscopy, BES, to reveal chemical composition changes with sub-micron spatial resolution has been explored by a number of authors [7]- [9]. Practical resolution appears to be only limited by the signal to noise ratio [10]. By breaking a

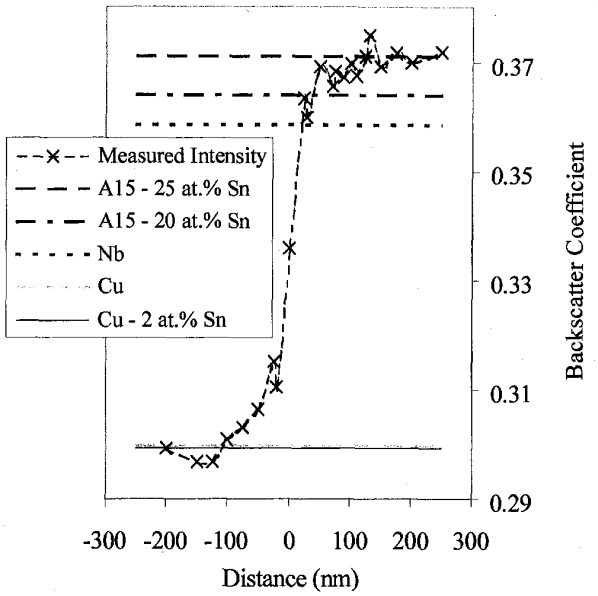

Fig. 2 Simulated backscatter traverse across depleted 2 atomic % Sn bronze (left) to stoichiometric A15 (right) boundary using 50,000 electrons per point. 100,000 electron simulated levels for bulk Cu, Nb, 25 atomic % Sn Nb_3Sn and 20 atomic % Sn Nb_3Sn are also shown.

conventionally obtained BEI image, into individual pixels and normalizing the positions of the pixels to the interfaces under study, we can combine signals from the entire image. For Nb_3Sn filaments with < 200 nm grain diameters, this approach also averages over multiple grain orientations, thus eliminating crystallographic back scatter yield variations. By Monte Carlo simulation [11] of the electron trajectories, the mean maximum depth of the backscattered electrons in Nb_3Sn is 40-50 nm for a 5 kV accelerating voltage. This rises

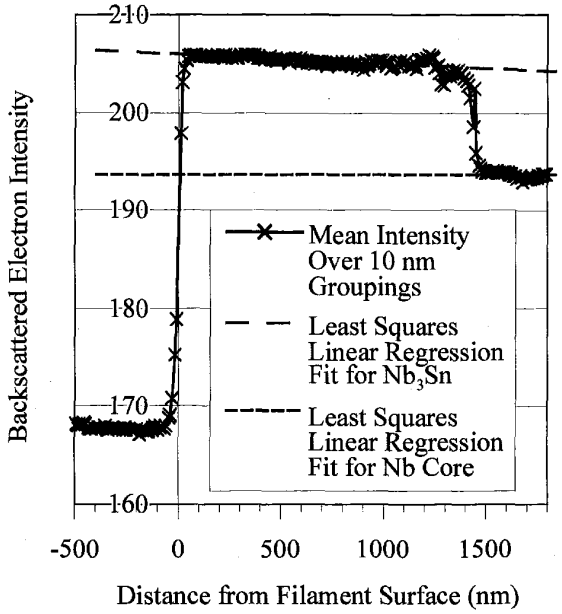

Fig. 3 Compositional variation across bronze process filament in a fully heat treated Vacuumschmelze ITER strand.

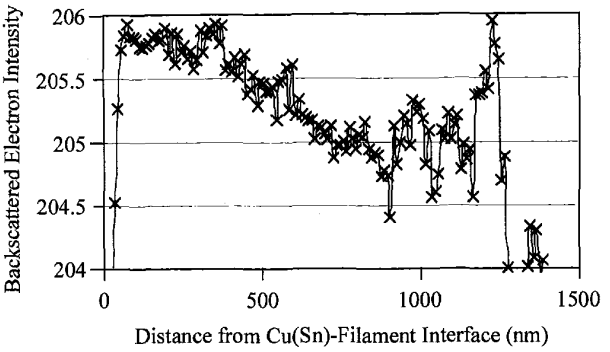

Fig. 4 Detail from the traverse in Fig. 3 showing a level backscatter intensity up to ~300 nm followed by a continuous drop until approximately 900 nm.

with accelerating voltage to over 180 nm at 12 kV. With the interfacial roughness indicated in Fig. 1c, it is important to keep the accelerating voltage as low as possible to obtain resolution on the sub-100 nm scale. A backscatter traverse across a depleted bronze to stoichiometric Nb_3Sn interface is shown in Fig. 2.

III. Results

A. Bronze Process ITER strand.

Fig. 3 shows the 5 kV electron backscatter variation across a bronze process filament. The gradient suggests a decline in Sn composition across the radius of the filament. The interface is as sharp as that simulated (Fig. 2) for a planar depleted bronze to 25 atomic % Sn A15 interface. The

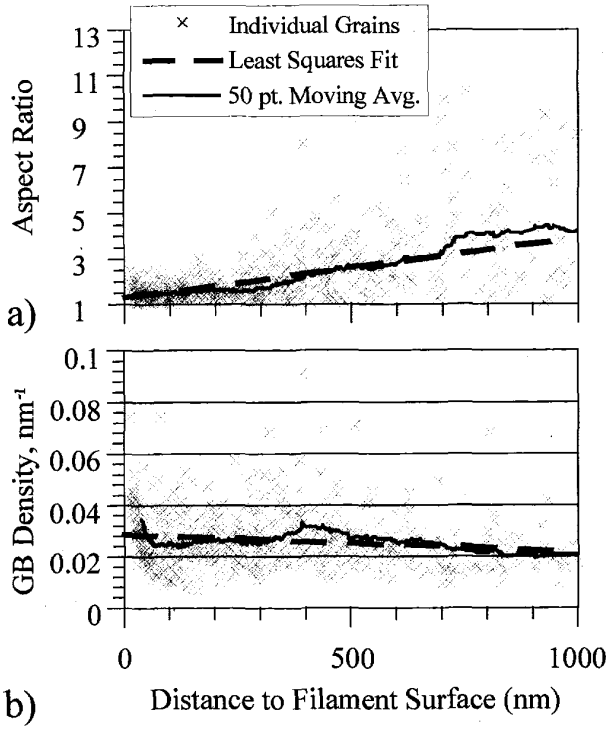

Fig. 5 a) Aspect ratio and b) grain boundary density change across filament radius for the strand in Fig. 3.

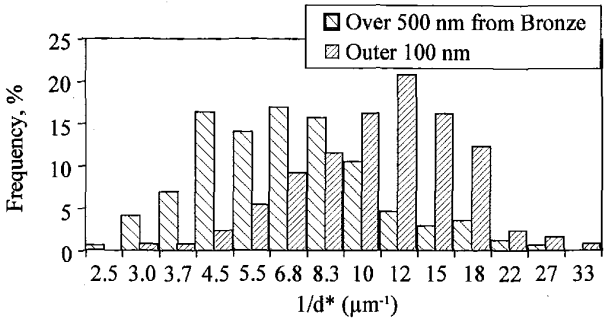

Fig. 6. Log normal distribution of inverse grain size, comparing outer 100 nm of radius with grains more than 500 nm from the bronze-A15 interface.

backscatter intensity across the A15 phase is shown in detail in Fig. 4. A flat intensity is observed over the first ~300-400 nm of the filament radius, followed by a continuous decline until approximately 900 nm from the bronze-filament interface.

In Fig. 5 the change in grain morphology (aspect ratio and grain boundary density) across the filament radius is shown. The aspect ratio is low for the first ~300 nm, after which there is a steady increase. The grain boundary density is highest near the filament surface, after which there is a plateau extending to ~300nm. After 300 nm there is a changeover which initially sees a spike in grain boundary density followed by a continuous decline.

The inverse grain size, 1/d, is often used as an indicator of F_{pmax}, in A15 superconductors, and allows comparison of this data with earlier work. In this work we calculate the diameter, d*, from the transverse cross-sectional area of the grain assuming it to be circular. The grain morphology has a relatively small impact on grain boundary density compared with d* and consequently the grain boundary density and 1/d* trends are almost identical even for filaments such as this with highly aspected grains. In Fig. 6, we contrast the distribution in 1/d for the outer, high-Sn 100 nm of the radius with that of the grains beyond 500 nm from the bronze, where BSE analysis indicates the Sn level is declining. As with the other measured microstructural features in Nb_3Sn [1](and Nb-Ti) the size distributions are best described as log-normal. The log-normal generated mean 1/d* for the outer 100 nm is 11.1 μm^{-1}, compared with a value of 6.7 μm^{-1} for the lower

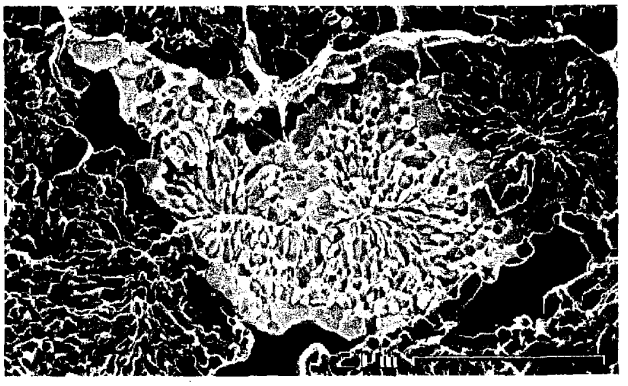

Fig. 7 FESEM fractograph detail from within the A15 layer in a high J_c, high Sn MJR strand. The original filaments are surrounded by a layer of large A15 grains. The highlighted filament is analyzed individually.

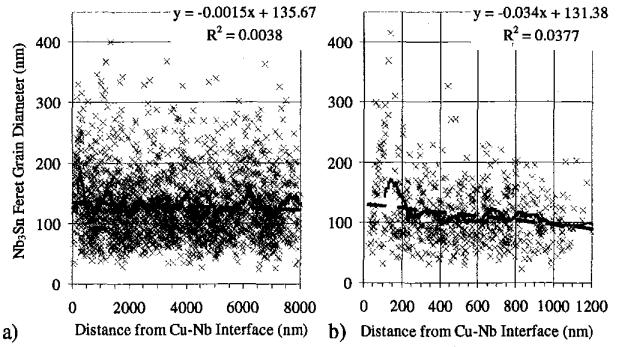

Fig. 8. Grain size variation a) across the coalesced A15 layer and b) across the original filament shown in Fig. 7. The dashed line is a least squares fit and the solid line is a 50 point moving average.

Sn interior (>500 nm from the bronze).

B. High Sn MJR internal Sn process strands.

Analysis of high-Sn, high-J_c, internal-Sn, MJR composites is complicated by the growing together of the filaments into a single filament mass. In Fig. 7 an original filament within the coalesced A15 layer of a high-Sn MJR composite is outlined. The microstructural variation across this layer (Fig. 8b) is strong compared with that averaged over the coalesced A15 layer (Fig. 8a).

A position normalized backscatter profile across the outer 4 μm of the reacted A15 layer is shown in Fig. 9. Although there is variability at the individual filament scale, the overall trace is flat.

C. High Sn source PIT strands.

ECN-type PIT filaments characteristically have a small interior layer of large grains surrounded by the main layer of fine grains. In Fig. 10 we show the grain size variation across the fine-grained A15 region in a PIT monofilament manufactured by Supercon. There is only a shallow gradient in grain size over the entire 20 μm layer.

IV. Summary

We now have the tools to provide a quantitative description of complex Nb_3Sn composites. These initial studies reveal important insights into the microstructural control of these strands. In a bronze-process strand we observe the onset of columnar growth simultaneously with a downturn in %Sn. In the high-Sn strand we observe that the principal variations are across the original filaments and not

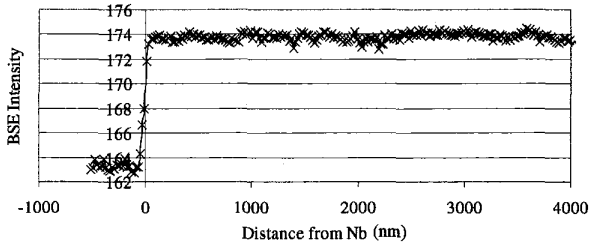

Fig. 9 Backscatter intensity across first 4 μm of A15 layer from Nb barrier in high Sn, high J_c, MJR strand.

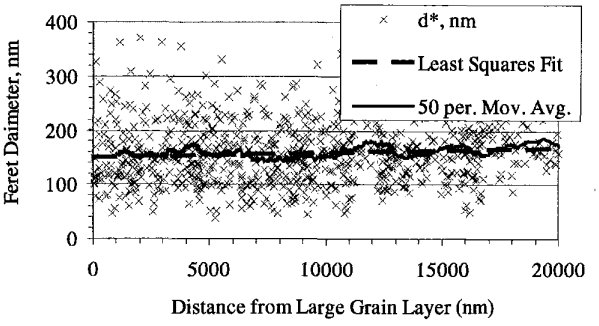

Fig. 10 Grain size variation across small grain Nb_3Sn layer in monofilament ECN-type PIT strand manufactured by Supercon.

across the coalesced filament pack. In the PIT strand, with a very high Sn content powder core, a uniform, and fine grain size can be achieved over a very long distance.

Acknowledgment

Internal Sn strand was provided by Oremet Wah Chang and by Seung Hong of OI-ST. Reacted monofilament PIT Nb_3Sn was supplied by Terrence Wong of Supercon. Processing and metallography at the UW was performed by William Starch, Danica Christensen, and Walid Gabr-Rayan.

References

[1] P. J. Lee, J. R. Ruess and D. C. Larbalestier, "Quantitative image analysis of filament coupling and grain size in ITER $Nb(Ti)_3Sn$ strand manufactured by the internal Sn process," *IEEE Trans. Applied Superconductivity*, vol. 7(2), pp. 1516-1519, 1997.

[2] K. R. Marken, S.-J. Kwon, P. J. Lee and D. C. Larbalestier, "Characterization studies of a fully reacted high bronze-to-niobium ratio filamentary Nb_3Sn composite," *Adv. Cryo. Eng. Materials*, 32, pp.967-975, 1986.

[3] R. Kimmich and P. Lee, "Microstructure of commercial Nb_3Sn-composites," internal report for Forschungszentrum Karlsruhe, Institut fuer Technische Physik, 1999.

[4] P. J. Lee, A. A. Squitieri and D. C. Larbalestier, "Nb_3Sn: macrostructure, microstructure, and property comparisons for bronze and internal Sn process strands," *IEEE Trans. on Applied Superconductivity*, 10(1), pp. 979-982, 2000.

[5] E. Gregory, E. Gulko, and T. Pyon, "Development of Nb_3Sn wires made by the internal-tin process, *Adv. Cryo. Eng. (Materials)*, 44, pp. 903-909, 1998.

[6] P. J. Lee and D. C. Larbalestier, "Position normalization as a tool to extract compositional and microstructural profiles from backscatter And Secondary Electron Images," Microscopy and Microanalysis, 6, Supplement 2, pp. 1026-1027, 2000.

[7] A. Konkol, G. R. Booker, P. R. Wilshaw, "Backscattered electron contrast on cross sections of interfaces and multilayers in the scanning electron microscope," *Ultramicroscopy*.58 (3-4), pp.233-7, June 1995.

[8] A. Konkol, "Resolution of compositional backscattered electron profiles of single interfaces in the scanning electron microscope," *Scanning*. 18(1), pp. 13-18, January 1996.

[9] D. R. Cousens and D. C. Joy, "A Monte Carlo study of the position of phase boundaries in backscattered electron images," *Scanning*, 19(8) pp 547-52, 1997.

[10] P. G. Merli, A. Migliori, M. Nacucchi, M. V. Antisari, "Comparison of spatial resolutions obtained with different signal components in scanning electron microscopy," *Ultramicroscopy*, 65(1-2), pp.23-30, 1996.

[11] P. Hovington, D. Drouin and R. Gauvin, "CASINO: A new Monte Carlo code in C language for electron beam interaction .1. Description of the program," *Scanning*, 19(1), pp. 1-14, January 1997.